Multiple fuel droplets evaporation effects on ambient conditions

Abgail P. Pinheiro*, João Marcelo Vedovoto, Marcelo M. R. Damasceno, Aristeu da Silveira Neto
School of Mechanical Engineering, Federal University of Uberlândia, Av. João Naves de Ávila, 2121, Bloco 5P, Uberlândia, Minas Gerais 38400-902, Brazil
*Corresponding author: abgail.pinheiro@gmail.com

Abstract
Multiple fuel droplets evaporation is investigated by means of three-dimensional numerical simulations performed in a in-house code. The purpose of this investigation is to study the processes of droplet evaporation and micro-mixing, which play a crucial role for fuel distribution in the gaseous phase. The mathematical model consists of balance equations in Lagrangian and Eulerian frameworks for liquid and gas phases, respectively. Based on the two-way coupling concept, a series of source terms accounting for mass, momentum and energy interactions between two phases are added to the balance equations of the gaseous phase. In order to validate the Lagrangian evaporation model, first, numerical simulations of a single droplet evaporation are performed and the results are compared to experimental data, afterwards, numerical simulations of multiple fuel droplets evaporation are performed for ambient temperature and pressure of 2000 K and 1 atm, respectively. The droplets are randomly distributed in the central region of a cubic domain as a spherical shape with a mass load ratio of 0.027. For all the simulations performed in this work, including the validation of the Lagrangian evaporation model and the two-phase flow simulations, n-decane is evaporated in a nitrogen gaseous medium. It is observed, as expected, that increasing the dispersed phase mass fraction decreases the ambient gas temperature and increases the ambient fuel vapor concentration; therefore, the droplet lifetime increases. The results finally reveal that the consideration of the two-way coupling in the mathematical model, even in the dilute case, could lead to some significant effects on the predictions of evaporation process.

Keywords
Droplet evaporation, Numerical simulation, Scalar gradients

Introduction

Evaporation of multiple droplets is a crucial factor for spray combustion simulation, since it determines the fuel vapor concentration available in the environment and, thus, influence the reaction rates [1]. For spray combustion simulations the Eulerian-Lagrangian approach is widely employed, especially for dilute spray simulations, where the mean inter-droplet spacing is larger than approximately ten droplet diameters. In the Lagrangian viewpoint, each individual droplet is tracked in its own frame of reference and ordinary differential equations are considered to determine their position, velocity, diameter and temperature temporal evolution. Point droplet approximation, which is assumed in the Lagrangian approach, is well justified for droplet sizes below the Kolmogorov length scale, as in the case studied in the present research. Meanwhile, the continuous phase is modeled by mass, momentum, energy and species balance equations computed based on the Eulerian viewpoint.
The evaporation of Lagrangian droplets deeply impacts the Eulerian variables spatial and temporal distributions [2], especially in the vicinity of the droplet surfaces. The mixing between the fuel vapor released by the evaporating droplets and the surrounding gaseous phase, and the energy transfer between gaseous and liquid phases are analyzed here. Scalar gradients of temperature and mixture fraction, or more specifically normalized mass fraction, are the main points observed. The purpose of the present study is to evaluate the effects of multiple droplets evaporation on the gaseous environment by means of three-dimensional numerical simulations. The evaporation of a droplet cloud with 0.027 liquid droplet mass loading ratio, which is the ratio of the total mass of fuel droplets to the mass of gas in the spherical region that contains the droplets, is simulated and its results are discussed.

Mathematical model

The present work is performed based on the Eulerian-Lagrangian framework, in which the continuous gaseous phase is modeled by the transport equations shown in the first part of this section. The dispersed liquid phase, based on Lagrangian referential is presented in the second part of this section. Finally, the coupling between the two phases is accounted by the transfer terms presented in the third part of this section.

Eulerian phase

The balance equations for of mass, momentum, energy and mass of each species are given by the following partial differential equations:

$$\frac{\partial u_i}{\partial x_i} = 0, \tag{1}$$

$$\frac{\partial \rho u_i}{\partial t} + \frac{\partial \rho u_i u_j}{\partial x_i} = -\frac{\partial p}{\partial x_i} + \frac{\partial \tau_{ij}}{\partial x_i} + {S_{u,i}}^L, \tag{2}$$

$$\frac{\partial \rho c_p T}{\partial t} + \frac{\partial \rho u_i c_p T}{\partial x_i} = \frac{\partial}{\partial x_i}\left(k\frac{\partial T}{\partial x_i}\right) + \rho\frac{\partial T}{\partial x_i}\sum_{k=1}^{N} c_{p,k} D_k \frac{\partial Y_k}{\partial x_i} + \tau_{ij}\frac{\partial u_i}{\partial x_j} + {S_{c_p T}}^L, \tag{3}$$

$$\frac{\partial \rho Y_k}{\partial t} + \frac{\partial \rho u_i Y_k}{\partial x_i} = \frac{\partial}{\partial x_i}\left(\rho D_k \frac{\partial Y_k}{\partial x_i}\right) + {S_k}^L, \tag{4}$$

where ρ is the density, u_i the gas velocity, p the pressure, τ_{ij} the viscous stress tensor, T the gas temperature, c_p the specific heat capacity capacity, k the thermal conductivity, and D_k and Y_k are the mass diffusion coefficient and the mass fraction of the kth species. ${S_{u,i}}^L$, ${S_{c_p T}}^L$ and ${S_k}^L$ are the momentum, energy and mass sources terms to account for the existence of the Lagrangian phase.

Lagrangian phase

The balance equations for of mass, momentum, energy of each individual droplet are given by the following ordinary differential equations:

$$\frac{dx_{d,i}}{dt} = u_{d,i}, \tag{5}$$

$$m_d \frac{du_{d,i}}{dt} = \sum F_{d,i}, \tag{6}$$

$$\frac{dm_d}{dt} = -\dot{m}_d, \tag{7}$$

$$m_d c_{p,l} \frac{dT_d}{dt} = \dot{Q}_s. \tag{8}$$

where x_d is the droplet position, u_d the droplet velocity, m_d the droplet mass, F_d the external forces acting on the droplet, $\dot{m}_d$ the droplet evaporation rate, $c_{p,l}$ the liquid droplet specific heat capacity capacity, T_d the droplet temperature, and $\dot{Q}_s$ the power transferred to promote the droplet thermal energy variation per unit of time, which is transferred as heat.

Based on a detailed analysis of different evaporation models [3], the Abramzon-Sirignano evaporation model (ASM) [4] is adopted to represent the mass and energy transfers, $\dot{m}_d$ and $\dot{Q}_s$, between the liquid and gaseous phases.

Phases coupling

The phase coupling between the gas and dispersed-droplets phases is calculated by a Particle-Source-In-Cell (PSI-Cell) method [5], and the source terms are given as:

Equation	${S_{dry}}^L$	${S_{wet}}^L$
Momentum	$\frac{1}{\Delta V}\sum_{d=1}^{N_d} m_d \left[\frac{\left({u_{d,i}}^{n+1} - {u_{d,i}}^{n}\right)}{\Delta t^{n+1}}\right]$	$\frac{1}{\Delta V}\sum_{d=1}^{N_d} {u_{d,i}}^{n}\dot{m}_d$
Species	0	$\frac{1}{\Delta V}\sum_{d=1}^{N_d} \dot{m}_d$
Energy	$\frac{1}{\Delta V}\sum_{d=1}^{N_d} \dot{Q}_s$	$\frac{1}{\Delta V}\sum_{d=1}^{N_d} \dot{m}_d(c_{p,v}T_d + L_v)$

where ΔV is the volume of the control volume for the gas phase calculation, Δt the time step, and L_v the latent heat of evaporation.

Numerical and computational model

ASM is implemented in the in-house code MFSim, under development at the Fluid Mechanics Laboratory (MFLab) at Federal University of Uberlandia and it is used for the simulations in this work. The 4th-order Runge-Kutta scheme is used for the time discretization of Eqs. (5) to (8) to predict the temporal advancement of droplet position, velocity, size and temperature. The physical properties for vapor and gas are obtained utilizing the open source Cantera software package [6], based on the phase molar composition and reference temperature at the gas-vapor mixture. Furthermore, the diffusivity of fuel vapor in gas, even when the gaseous phase is a mixture, is also directly calculated by Cantera as a function of molar composition, reference temperature and ambient pressure. It is worthy noting that by using Cantera the evaluation of thermal and transport properties is greatly facilitated, once such parameters are evaluated from a single source of data, i.e., a single cti file of the fluids of interest. The liquid droplet properties, ρ_l and c_{pl}, the latent heat of evaporation, and the saturated vapor pressure are calculated based on the database found in Green and Perry [7]. Finally, all the thermodynamic and transport properties for liquid, vapor and gas phases are assumed constant during each time step, but they vary from one time step to another due to the corresponding changes in droplet temperature.

For a numerical approximation of the gas phase, the partial differential equations were discretized with a standard finite volume method. Velocity–pressure coupling was accomplished by using a semi-implicit fractional step projection method. The CUBISTA scheme is used for the spatial discretization of the advective terms, while central difference scheme is retained for all others spatial derivatives. All the linear systems in are solved implicitly using a multigrid-multilevel solver. As boundary conditions, on all six boundaries, the free outflow condition is adopted.

Figure 1 shows the schematic representation of the three-dimensional, Cartesian grid, computational domain and the initial droplet random distribution. The computational domain is a cube 5 mm on a side and is divided into 64 computational grid points in each direction. The multiple fuel droplets are allocated at the center of the cubic computational domain and in the central region as a spherical shape with 4 mm diameter.

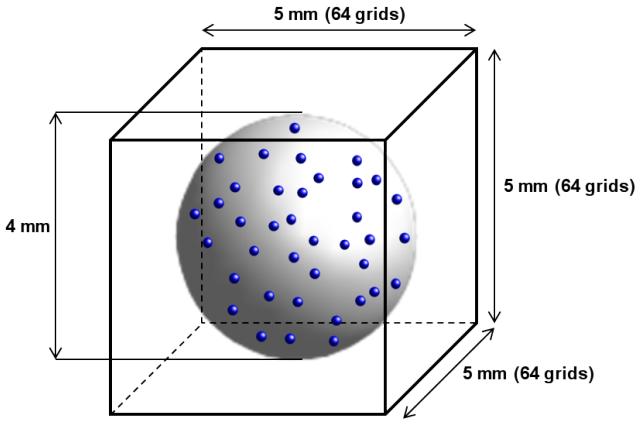

Figure 1. Computational domain schematic illustration

Results and discussion

Evaporation model validation

In order to validate the theoretical model predictions, the evaporation rate of a single n-decane droplet is calculated under the assumption that the variations of the gas temperature and mass fraction of fuel gas caused by the droplet evaporation are negligible small, and the results are compared against experimental measurements. Wong and Lin [8] present experimental data for a test case of n-decane droplet with initial diameter D_{do} = 1.961 mm and temperature T_{do} = 315 K evaporating in air at T = 1000 K and p = 0.1 MPa. The stationary droplet is in an air environment with u = 1.0 m/s. In their experiment, the temperature of evaporating decane droplets was measured with a thermocouple.

In Figure 2a, the normalized squared droplet diameter temporal evolution measured by Wong and Lin [8] and predicted by ASM model are shown. In Figure 2b, the associated droplet temperature temporal evolution with the wet-bulb temperature for the case, T_{wb} = 420 K, is presented. As it can be noticed by those figures, the droplet equilibrium temperature reached in the experiment is higher than the one simulated, resulting in an experimental droplet lifetime smaller than the one simulated. Even though Sherwood and Nusselt empirical correlations might be used by comparing them with the values computed by ASM, those correlations are not used in this validation because, for the best knowledge of the authors, there is no correlation available that properly represents cases of laminar regime and high Spalding transfer number as the case presented here, whose Re_d = 17, B_T = 5.7, and B_M = 4.5.

Since Wong and Lin [8] experiment was performed using the classical single fiber technique, their results may have been influenced by the extra energy transfer from the fiber to the droplet through conduction. This extra energy transfer would increase the droplet equilibrium temperature and, as a consequence, decrease the droplet lifetime.

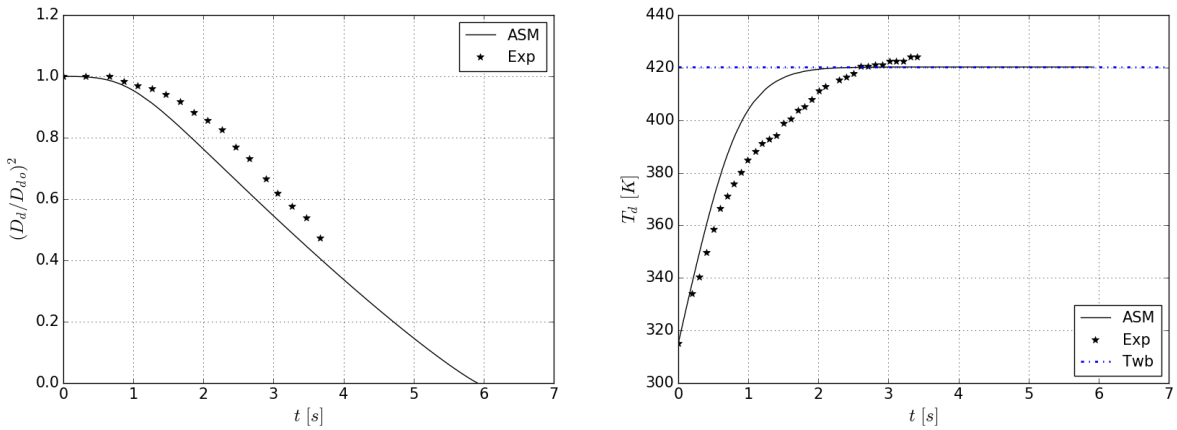

(a) Normalized squared droplet diameter

(b) Droplet temperature

Figure 2. Comparison between experimental and simulated data for n-decane droplet evaporation.

With this extra energy transfer present, the droplet temperature would gradually increase instead of remaining at the wet-bulb temperature, as explained by Wong and Lin [8].

Multiple droplets evaporation

This section presents the simulation results of a group of n-decane droplets, with initial diameter D_{do} = 7.5 μm and temperature T_{do} = 300 K, evaporating in nitrogen at initial gas temperature T_o = 2000 K and ambient pressure p = 0.1 MPa. The stationary droplets are placed in an quiescent medium. The present simulation has a droplet mass loading of 0.027, resulting in 120 droplets.

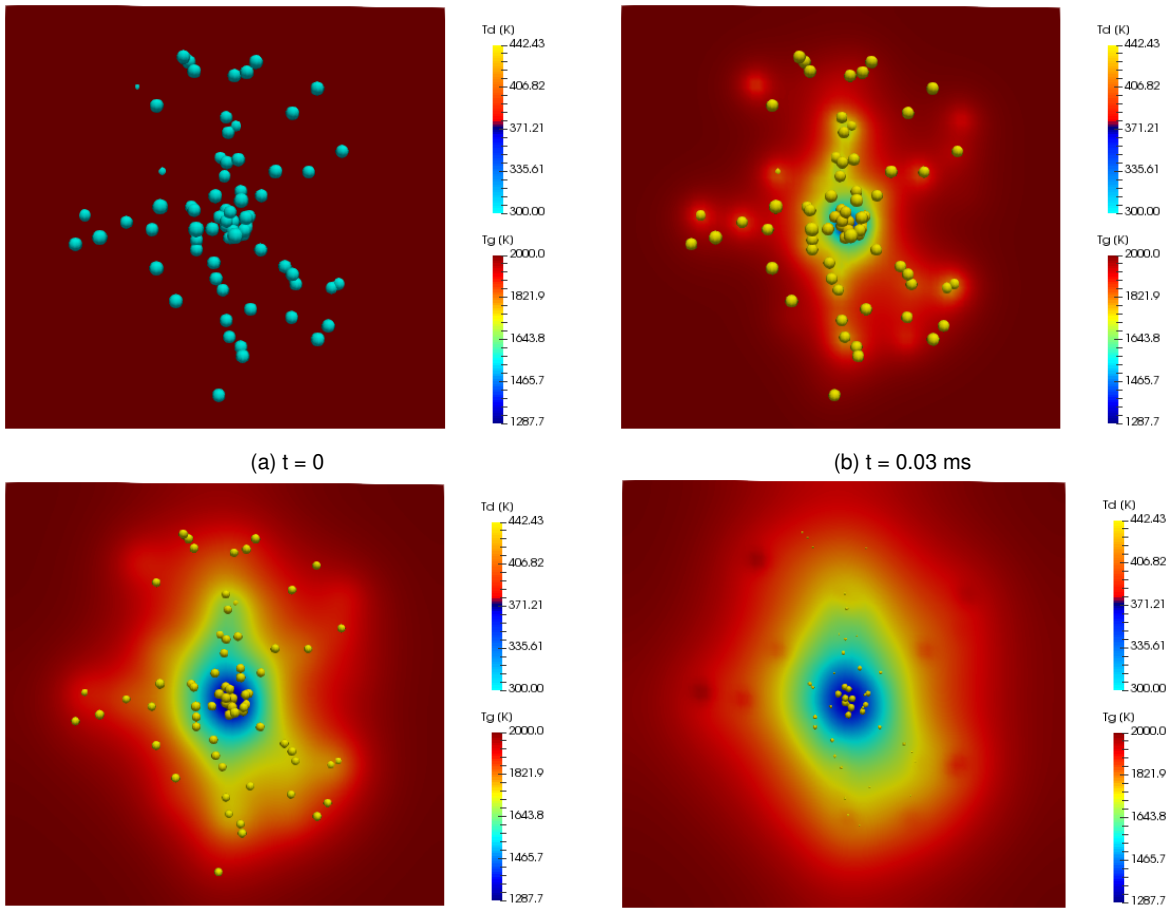

(a) t = 0

(b) t = 0.03 ms

(c) t = 0.06 ms

(d) t = 0.09 ms

Figure 3. Time variations of distributions of instantaneous gas temperature.

Figure 3 shows the time variation of instantaneous gas temperature, T, distribution and droplet temperature, T_d,

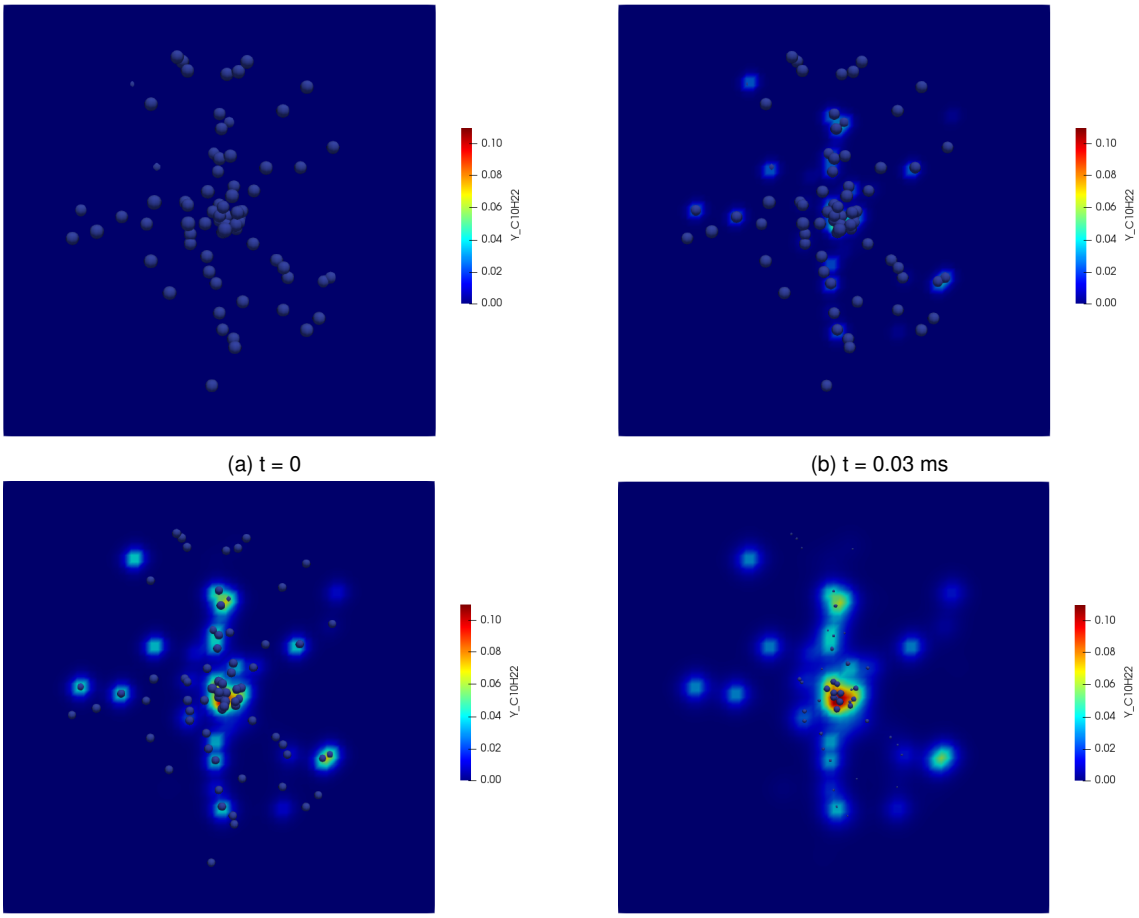

(a) t = 0 (b) t = 0.03 ms

(c) t = 0.06 ms (d) t = 0.09 ms

Figure 4. Time variations of distributions of instantaneous fuel gas mass fraction.

while Figure 4 shows the evaporated fuel mass fraction distribution, Y_v. The n-decane evaporation enhances its ambient mass fraction, which act to suppress the droplet evaporation and therefore enlarge the droplet lifetime. Furthermore, since the liquid droplet needs heat to increase its temperature and, then, evaporate, the gaseous medium transfer this energy, which is reflected as the ambient temperature decrease. Both droplet and gas velocities are zero in the present simulation. Therefore, vapor mixing occurs only by diffusion due to the existing mass fraction gradients.

As expected in the central region, where there is a droplet cluster, the evaporation rate is smaller, since the fuel vapor concentration in the continuos phase is higher is this region. In the beginning of the simulation, the ambient fuel vapor mass fraction is zero for all the Eulerian cells that represent the continuos phase, as it can be seen in Figure 4a. Once the energy transfer begins, and, hence, the evaporation process, the ambient fuel vapor mass fraction increases, causing a decrease in the evaporation rate. Moreover, the evaporation rate also decreases because the ambient temperature decreases as the evaporation process occurs, as shown in Figure 3. On the other hand, the peripheral droplets evaporate faster than those at the center region, even though that have the same initial diameter. This difference between peripheral and central droplets evaporation is due to the effect of cluster evaporation. Peripheral droplets evaporation have a similar behavior to those of isolated droplets, since their influence on the variations of the ambient temperature and fuel vapor mass fraction is small.

In Figure 5, Eulerian variables spatial distribution in the domain centerline are presented. First, in Figure 5a, it is shown that in the beginning of the simulation all the Eulerian variables are constant, since the initial condition is T_o = 2000 K, Y_{N_2} = 1, and $Y_{C_{10}H_{22}}$ = 0 for the entire domain. As the evaporation process happens, the domain temperature changes due to energy and mass transfers. The nitrogen and n-decane mass fractions show that where the evaporation occurs, the fuel mixture fraction increases, and that the sum of both mass fractions results in unity, as expected. For x = 2.5 mm, at the domain central point, the maximum evaporation rate is observed, due to the droplet concentration in this point, which results in the domain lowest temperature and highest fuel vapor concentration. The others images show some properties of the ambient mixture, such as specific heat capacity, density, viscosity and thermal conductivity, based on the ambient gas temperature and composition computed throughout the simulation.

Conclusions

It is observed, as expected, that increasing the dispersed phase mass fraction decreases the ambient gas temperature and increases the ambient fuel vapor concentration; therefore, the droplet lifetime increases. The results finally

reveal that the consideration of the two-way coupling in the mathematical model, even in the dilute case, could lead to some significant effects on the predictions of evaporation process.

Acknowledgements
The authors thank the financial and technical support from Petróleo Brasileiro S.A. (Petrobras), National Counsel of Technological and Scientific Development (CNPq), Minas Gerais State Agency for Research and Development (FAPEMIG) and Coordination for the Improvement of Higher Education Personnel (CAPES) - Finance Code 001.

Nomenclature

ΔV	volume of the control volume [m^3]
Δt	time step [s]
μ	dynamic viscosity [kg/(m s)]
ρ	density [kg/m^3]
τ_{ij}	viscous stress tensor [kg/(m s^2)]
c_p	specific heat capacity [J/(kg K)]
D_d	droplet diameter [m]
D_k	binary diffusion coefficient of the kth specie [m^2/s]
F_d	external forces acting on the droplet [N]
k	thermal conductivity [J/(m s K)]
L_v	specific latent heat of evaporation [J/kg]
m_d	droplet mass [kg]
$\dot{m}_d$	droplet mass evaporation rate [kg/s]
p	pressure [Pa]
Q_S	sensible energy per unit of time [J/s]
${S_{u,i}}^L$	momentum coupling source term [kg/(m^2 s^2)]
${S_{c_pT}}^L$	energy coupling source term [kg/(m s^3)]
${S_k}^L$	specie mass fraction coupling source term of the kth specie [kg/(m^3 s)]
T	gas temperature [K]
T_d	droplet temperature [K]
u_d	droplet velocity [m/s]
u_i	gas velocity [m/s]
x_d	droplet position [m]
Y_k	mass fraction of the kth specie [-]

References

[1] Jenny, P.; Roekaerts, D.; Beishuizen, N. Modeling of turbulent dilute spray combustion. *Progress in Energy and Combustion Science*, v. 38, n. 6, p. 846 – 887, 2012.

[2] Kitano, T.; Nishio, J.; Kurose, R.; Komori, S. Effects of ambient pressure, gas temperature and combustion reaction on droplet evaporation. *Combustion and Flame*, v. 161, n. 2, p. 551 – 564, 2014.

[3] Pinheiro, A. P. and Vedovoto, J. M. (2018). Evaluation of droplet evaporation models and the incorporation of natural convection effects. *Flow, Turbulence and Combustion*.

[4] Abramzon, B. and Sirignano, W. (1989). Droplet vaporization model for spray combustion calculations. *International Journal of Heat and Mass Transfer*, 32(9):1605–1618.

[5] Crowe, C. T.; Sharma, M. P.; Stock, D. E. The Particle-Source-In Cell (PSI-CELL) model for gas-droplet flows. *Journal of Fluids Engineering*, ASME, v. 99, p. 325– 332, 1977.

[6] Goodwin, D. G., Moffat, H. K., and Speth, R. L. (2016). Cantera: An object-oriented software toolkit for chemical kinetics, thermodynamics, and transport processes. Version 2.2.1.

[7] Green, D. W. and Perry, R. H. (2007). *Perry's Chemical Engineers' Handbook*. McGraw-Hill, New York, USA, 8 edition.

[8] Wong, S. C.; Lin, A. C. Internal temperature distributions of droplets vaporizing in high-temperature convective flows. *Journal of Fluid Mechanics*, Cambridge University Press, v. 237, p. 671–687, 1992.

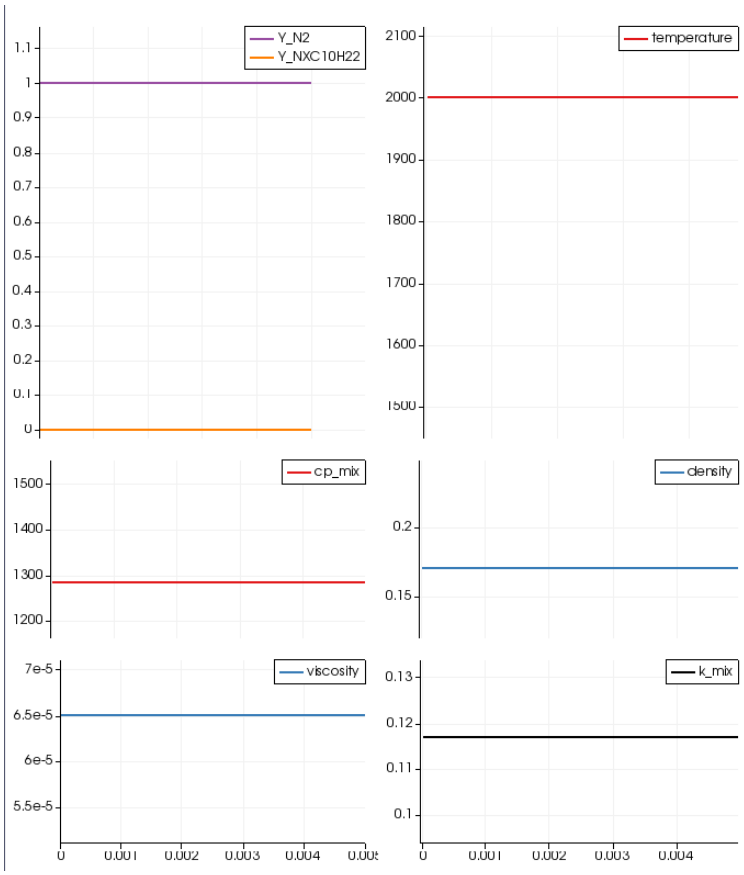

(a) t = 0

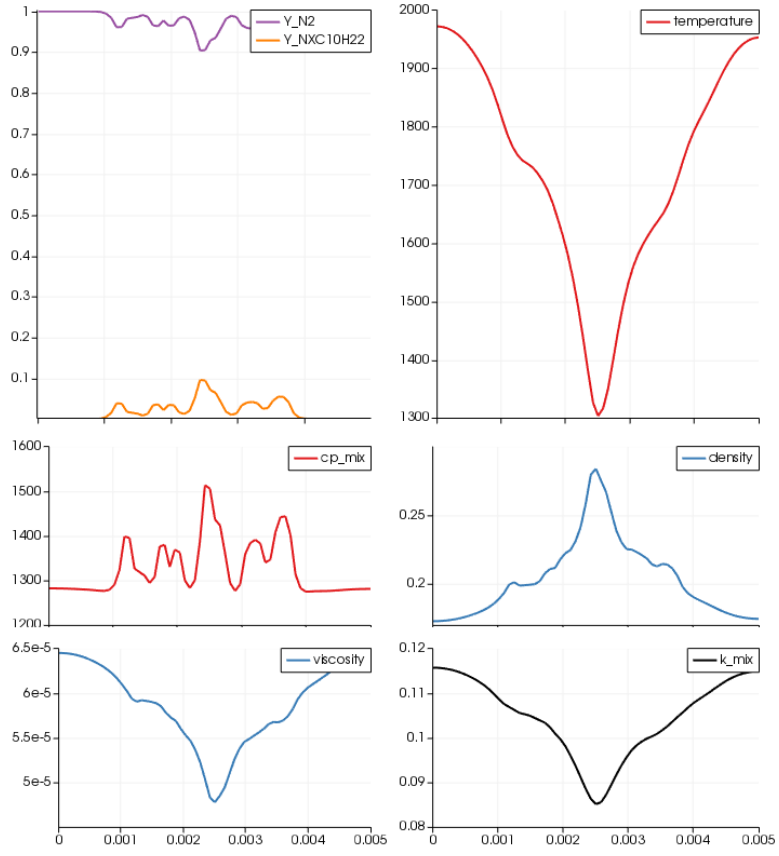

(b) t = 0.065 ms

Figure 5. Spatial variations of specific heat capacity, density, viscosity and thermal conductivity at the domain centerline due the ambient temperature and composition changes.